The Meteoritical Society

Meteoritics & Planetary Science 43, Nr 1/2, 335–351 (2008)
Abstract available online at http://meteoritics.org

Characterization of carbon- and nitrogen-rich particle fragments captured from comet 81P/Wild 2

J.-P. GALLIEN[1], H. KHODJA[1], G. F. HERZOG[2*], S. TAYLOR[3], E. KOEPSELL[4], C. P. DAGHLIAN[4], G. J. FLYNN[5], I. SITNITSKY[5], A. LANZIROTTI[6], S. R. SUTTON[6,7], and L. P. KELLER[8]

[1]Laboratoire Pierre Süe, CEA-CNRS, CEA Saclay 91191, Gif-Sur-Yvette, Cedex, France
[2]Department of Chemistry and Chemical Biology, Rutgers University, 610 Taylor Road, Piscataway, New Jersey 08854–8087, USA
[3]CRREL, 72 Lyme Road, Hanover, New Hampshire 03755, USA
[4]Dartmouth College, Hanover, New Hampshire 03755, USA
[5]Department of Physics, SUNY-Plattsburgh, 101 Broad Street, Plattsburgh, New York 12901–2681, USA
[6]Consortium for Advanced Radiation Sources, University of Chicago, Chicago, Illinois 60637, USA
[7]Department of the Geophysical Sciences, University of Chicago, Chicago, Illinois 60637, USA
[8]NASA Johnson Space Center, Houston, Texas 77058, USA
[*]Corresponding author. E-mail: gherzog@rci.rutgers.edu

(Submitted 18 January 2007; revision accepted 08 August 2007)

Abstract–We studied three Stardust fragments with infrared spectroscopy to characterize organic matter; with synchrotron-induced X-ray fluorescence to determine Fe contents and certain elemental ratios to iron; with scanning electron microscopy (SEM) to image sample morphology and to detect semiquantitatively Mg, Al, Si, Ca, and Fe; and with nuclear reaction analysis (NRA) to measure C, N, O, and Si. A fourth fragment was analyzed by SEM only.

Fragment C2054,0,35,21 from track 35 (hereafter C21) is extremely rich in C and contains appreciable concentrations of Mg, Al, and Ca, but little Fe. Fragments C2054,0,35,23 (C23), C2044,0,41 (C41), and C2054,0,35,51,0 (C51), from tracks 35, 41, and 35, respectively, consist largely but not exclusively of aerogel. C23 contains Mg and finely dispersed S, but little Al, Ca or Fe. Pooled CI-normalized elemental ratios for C21, C23, and C41 are as follows: Ti/Fe, 5.0; Cr/Fe, 0.84; Mn/Fe, 0.97; Ni/Fe, 2.4; and Zn/Fe, 31. The enrichments in Ti and Zn may be related to the presence of aerogel.

Minimum weight percentages of C and N estimated without correcting for the presence of aerogel are 30 and 0.7 for C21; 2.8 and 0.2 for C23; 1.2 and 0.14 for C41. After corrections for the presence of aerogel containing 1.4 wt% C and 0.02 wt% N, the corresponding results are 37 and 0.85 for C21; and 10 and 1 for C23; and ~1 and ~1, for C41 (The results for C41 have large uncertainties). These weight percentages are larger than or comparable to values for carbonaceous meteorites. C/N atomic ratios without/without aerogel corrections are 51/51 for C21, 17/11 for C23, and 10/~1 for C41. Within the uncertainties these values are within the range for carbonaceous meteorites.

INTRODUCTION

The Stardust mission brought back material from comet 81P/Wild 2 for laboratory study. Carbon and nitrogen in this documented material are of interest for several reasons. First, they are the principal components of the "organic" phase(s) known from remote observations in many comets (A'Hearn et al. 1995; Jessberger and Kissel 1991). Second, the absolute and/or relative abundances of carbon and nitrogen may have taxonomic significance (Brownlee 2004). Third, in the inner part of the early solar system carbon helped determine the oxygen fugacity and hence the oxidation state of many elements (Larimer 1968). By extension, if unaltered since formation, the abundance of carbon in cometary grains may be a useful indicator of redox conditions in the regions where comets formed. Fourth, an early cometary bombardment of Earth may have introduced significant masses of carbon and nitrogen, thereby influencing atmospheric composition, surface temperatures (through the greenhouse effect), and even the evolution of life (Chyba and Sagan 1992; McKay and Borucki 1997; Oró 2000; Dauphas 2003). Knowledge of carbon and nitrogen concentrations in representative comets could help in estimating the incoming mass flux of these elements.

Table 1. Methods of analysis[a] and measurements.

Samples	Measurement	Method	Purpose
Indium foils	Elemental analysis	SXRF	Check background for $Z \geq 16$
Validation samples	C, N	NRA	Check nuclear reaction method
Stardust fragments	Vibrational spectra	IR spectroscopy	Identify C-rich fragments and functional groups
	C, N	NRA	Determine C and N contents and C/N ratios
	Fe	DXRF	Cross check with SXRF
	Elemental analysis[b]	SXRF	Characterize fragments
	Elemental analysis/petrography	SEM-EDAX	Characterize fragments

[a]SXRF = synchrotron-induced X-ray fluorescence. NRA = nuclear reaction analysis. DXRF = deuteron-induced X-ray fluorescence. SEM-EDAX = scanning electron microscopy with energy-dispersive X-ray detection.
[b]SXRF analyses of C21 and C23 were performed before NRA analyses and of C41 after NRA analysis.

Prior to the return of Stardust to Earth, remote spectroscopy and time-of-flight mass spectrometry during encounter had held out the promise that the particles from Wild 2 might be rich in carbon and nitrogen (Kissel et al. 2004; Farnham and Schleicher 2005). Even so, it seemed likely that the size of Stardust materials would pose challenging analytical problems. Inspection of the aerogel capture cells confirmed this expectation. Small to begin with, the cometary particles broke into still smaller fragments as they slowed in aerogel, spreading their mass over "tracks," typically less than 200 μm long but ranging upward to 21.9 mm (Hörz et al. 2006). (Below, we maintain a distinction between the primary, intact *particles* on the one hand and secondary *fragments* on the other.)

With cometary fragments so small and total masses limited, analytical methods of great sensitivity that affect samples minimally are preferred. Electron energy loss spectroscopy (EELS) and X-ray absorption near edge structure (XANES) allow the determination of carbon and nitrogen in surfaces no thicker than a few hundred nanometers. While EELS and XANES are effectively non-destructive, the measurements may not represent adequately the "bulk" composition of a sample. Secondary ion mass spectrometry of carbon and nitrogen has the sensitivity needed to analyze a surface layer, but questions of representativeness arise again.

The use of nuclear reaction analysis (NRA) for the determination of N dates to the late 1960s (see, e.g., Simpson and Earwaker 1986). A specific application of the $^{14}N(d,po)^{15}N$ reaction to extraterrestrial samples was described in the mid 1980s (e.g., Herzog et al. 1985) but was not developed. Starting in the early 1990s, scientists at Saclay (and elsewhere) devised quantitative ion beam techniques aimed primarily at carbon and nitrogen (Mosbah et al. 1993; Varela et al. 2003; Gallien et al. 2004). Matrajt et al. (2003) exploited this capability by measuring carbon and nitrogen in carbonaceous chondrites and several IDPs and demonstrated its utility for samples with sub microgram masses. Mainly on the strength of this work, we decided to use the same method to measure the total numbers of carbon and nitrogen atoms in fragments from comet Wild 2. We counted among its potential disadvantages the possibility that deuteron irradiation would activate the samples and change isotopic ratios to a measurable extent. In principle, extended irradiation could also cause radiation damage, although no evidence for this effect in crystalline materials has emerged from studies carried out over many years at the Saclay laboratories.

In light of the importance of the Stardust samples, it seemed desirable to obtain as much petrographic and compositional information as possible about the fragments. Accordingly, we imaged the samples using the SEM at Dartmouth and the X-ray fluorescence microprobe at Brookhaven's National Synchrotron Light Source.

The protocol of the Preliminary Examination Team required the validation of all methods through the analysis of "known" samples. We include here the results of those studies.

EXPERIMENTAL METHODS

Table 1 summarizes the flow of work in roughly the order it was carried out. The analytical method for carbon and nitrogen requires vertical mounting of samples in vacuum on a conductive medium. We chose indium for its softness, purity, and ready availability. In preliminary studies, indium foils (99.999%; 0.1 mm thick; Goodfellow) give rise to a manageable X-ray fluorescence background for the elements Ti, Cr, Mn, Fe, Ni, and Zn (Herzog et al. 2006). Backgrounds due to indium L X-rays were problematic for the detection of K X-rays from calcium and potassium.

We selected validation samples with known carbon and nitrogen contents; stability under the experimental conditions, where some heating was expected; and/or properties similar to those anticipated for the cometary particles. Three chemical reagents containing carbon and nitrogen as major elements seemed suitable: sodium cyanate (NaOCN), potassium cyanate (KOCN), and tripotassium hexacyanoferrate ($K_3Fe(CN)_6$). NaOCN decomposes at 700 °C; KOCN decomposes at 700–900 °C; and although $K_3Fe(CN)_6$ starts to decompose in vacuum at 200 °C, its C/N ratio remains constant up to ~420 °C (Wang et al. 1986).

For comparison with the previous results from both the literature and from NRA (Matrajt et al. 2003), we also

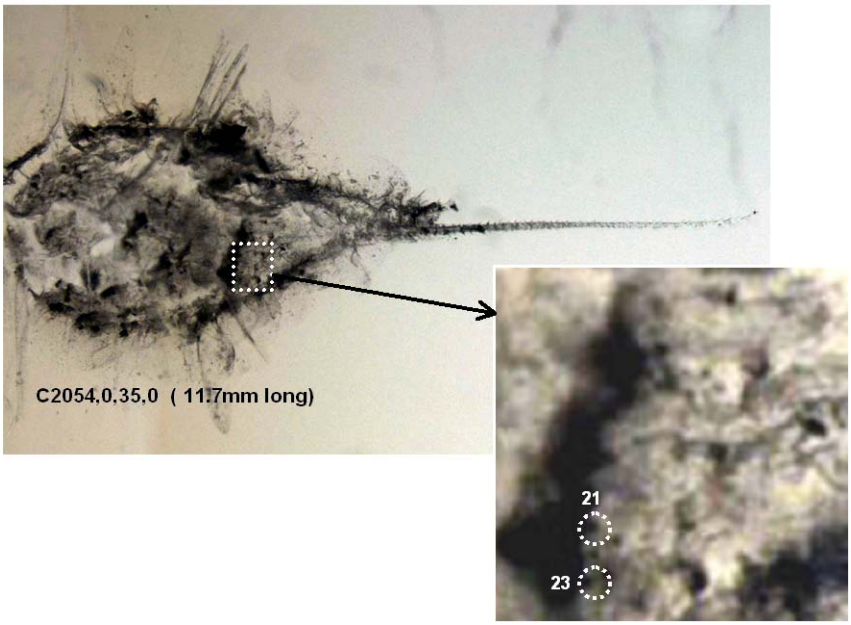

Fig. 1. Bulbous track 2054,0,35 (~11.7 mm long). Enlarged region shows the original locations of two of the particles studied, C21 and C23.

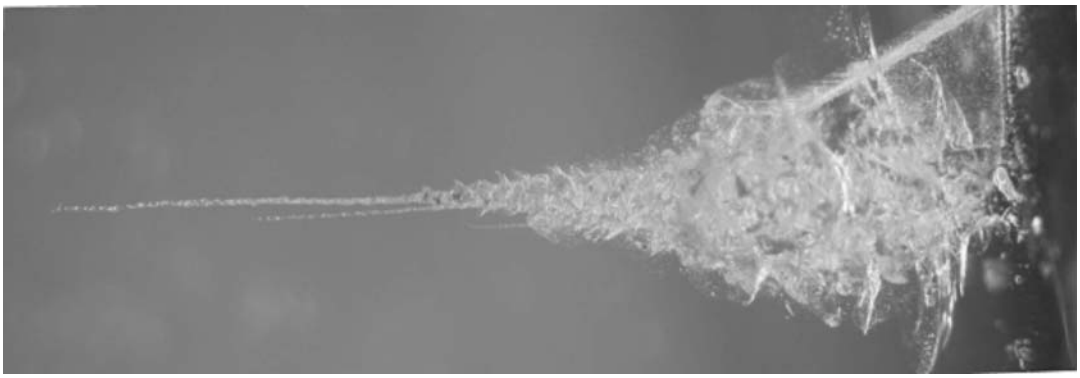

Fig. 2. Track 41 with keystone partially removed.

decided to analyze two relatively fine-grained, carbon-rich meteorites, namely, the carbonaceous chondrites Murchison and Tagish Lake. The meteorite samples were ground lightly in an agate mortar and pestle. A few grains were transferred with a brush to an indium foil and pressed into the foil with an aluminum disk.

Selection of Stardust Fragments for Analysis

Soon after the Stardust mission's return, the first maps of tracks made from X-ray fluorescence data revealed highly non-uniform distributions of the elements with $Z \geq 16$ (Flynn et al. 2006). Similarly, maps "in" the infrared implied large relative variations in the concentrations of C (Sandford et al. 2006). Given this information and our reluctance to report only upper limits, we requested as our first samples fragments likely to be rich in carbon and nitrogen. Results from infrared studies helped guide the selections.

Lindsay Keller and Keiko Messenger extracted the two fragments C2054,0,35,21 (hereafter C21) and C2054,0,35,23 (hereafter C23) from the wall of Track 35 (Fig. 1). Both fragments were quite dark in appearance and relatively large in area, ~250 μm^2. Andrew Westphal and Christopher Snead selected the third fragment from the wall of track 41, C2044,0,41 (hereafter C41), on the basis of size and color (Fig. 2). Its original size area was ~250 μm^2, but part of this fragment was lost during nuclear reaction analysis. Finally, we received a potted butt containing a fragment from Track 35, C2054,0,35,51,0 (hereafter C51), which was analyzed by SEM only. Its area was approximately 150 μm^2.

Selection of Aerogel Fragments

We had anticipated, naively as it turned out, that our Stardust fragments would contain little aerogel and that associated blank corrections for C and N would be small. In

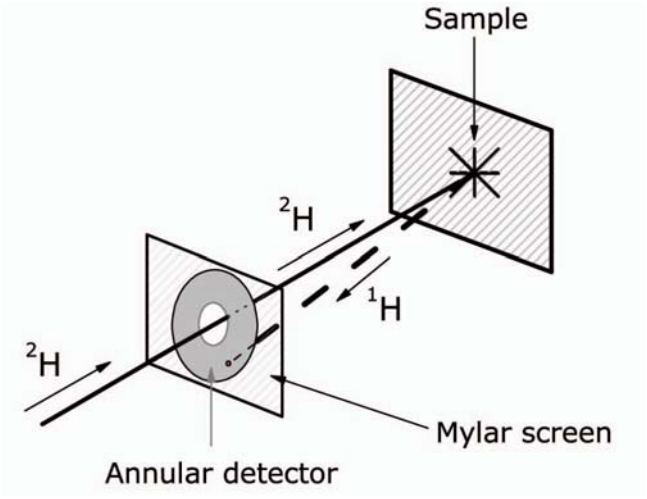

Fig. 3. Schematic diagram of the nuclear reaction analysis method.

fact, two of our Stardust fragments contained appreciable amounts of wholly or partially melted aerogel. We therefore analyzed portions of three samples of flight-quality aerogel. Aerogel samples 1 and 4 came to us directly from the Johnson Space Center courtesy of Michael Zolensky. Two portions from Aerogel 1 were pressed into indium at the Johnson Space Center and a third one at Dartmouth College. All three of these portions were examined by scanning electron microscopy prior to nuclear reaction analysis. Denton Ebel shared with us a sample of Aerogel 3, which he had in turn received from Fred Hörz (Johnson Space Center). We received separately an intact block of aerogel, Aerogel 4 (W12TZ), while at Saclay, where we cut off a small piece, which we pressed into indium and mounted for immediate analysis.

Infrared Spectroscopy

For Fourier transform infrared (FTIR) measurements, grains C21 and C23 were placed on CVD (chemical vapor deposition) diamond. Transmission FTIR spectra were collected using a Nicolet Nexus 670 Fourier-transform infrared spectrometer bench, interfaced with a Nicolet Continuum IR microscope and a LabSphere external integrating sphere. Solid state detectors and beam splitters cover the wavelength range from 4000 cm^{-1} to 650 cm^{-1}. The FTIR aperture was adjusted to the size of the particles, typically ~20 μm. The samples and the microscope were continuously purged with dry N_2. Background spectra were acquired from the substrate immediately adjacent to the sample. Final spectra were obtained by subtracting the background from the sample spectra and then smoothing. A total of 1024 scans (interferograms) with a spectral resolution of 4 cm^{-1} were averaged for each specimen. Detection limits for different functional groups vary with mass, band strengths, spectral overlap and other factors, but are typically in the percent range.

Mounting of Fragments for Nuclear Reaction Analysis

Random portions of aerogel were pressed into indium with either a glass slide, an aluminum disk, or with tweezers. Fragments C21 and C23 were pressed into one indium foil after IR spectroscopy and fragment C41 was pressed into a second one. Each foil with its embedded fragment(s) was attached to a 1-inch aluminum mounting disk either by pressing the foil onto the disks with a second piece of cleaned Al, with care taken to avoid touching the fragments, or with adhesive tape placed along the edge of the foil.

Nuclear Reaction Analysis and Deuteron-Induced X-Ray Fluorescence

We measured C, N, O, and Si in aerogel samples and in C21, C23, and C41 by using the nuclear method developed at Saclay (Mosbah et al. 1993; Varela et al. 2003; Gallien et al. 2004) and shown schematically in Fig. 3. For a fixed irradiation energy, the thickness of sample probed by the deuteron beam varies inversely with the sample density. Detailed calculations show that for a sample consisting mainly of silica (density 2.3–2.6 g/cm^3) the counting rates due to uniform, trace concentrations of carbon and nitrogen increase linearly to a depth of approximately 15 μm. Using the relevant nuclear cross sections, we estimated the degree to which the deuteron irradiation affected the isotopic composition of carbon: it is less than 1 ppm. Most deuterons deposit very little energy in the sample and consequently we expect radiation damage to have been minimal.

A small particle accelerator generates a tightly focused (2 μm × 2 μm) deuteron beam with an energy of 1.9 MeV and a current of ~0.5 nA. On striking a target, the beam induces the nuclear reactions $^{12}C + {}^2H \Rightarrow {}^{13}C + {}^1H$ ($^{12}C(d,p)^{13}C$) and $^{14}N + {}^2H \Rightarrow {}^{15}N + {}^1H$ ($^{14}N(d,p)^{15}N$) among others. Nuclear reactions that lead to the ground states of ^{13}C and ^{15}N produce protons with a characteristic, maximum energy of 3.5 MeV and 8.9 MeV, respectively.

The observed proton spectra consist of peaks of varying width partly because the emitted protons lose energy as they pass through the target on their way to the detector, and partly because of a background created by unresolved nuclear reactions. By rastering the beam across the surface of the target we were able to determine the spatial distribution of carbon and nitrogen with a resolution of about 2 μm. Data acquisition took about 12 hours for each fragment. During each analysis we monitored various X-ray maps of the sample, recentering when necessary.

Proton energy spectra for unknowns were converted to numbers of atoms through fitting procedures that incorporate cross sections from the SIMNRA data base and proton spectra measured for the following laboratory standard materials: SiO_2, Al_2O_3, UO_2, FeS_2, $CaCO_3$, and TiN. During an early stage of the analysis, a portion of fragment C41 was lost from the indium foil for unknown reasons. The data for the lost portion

of the sample are not included in the quantitative results below but were similar to them.

A separate detector in the reaction chamber was used to monitor X-rays stimulated in the sample by the deuteron beam. The X-ray spectra provide independent information about the iron concentrations in the sample.

SXRF

X-ray fluorescence (XRF) analyses of selected elements were made for all three fragments by using the X-ray microprobe of Brookhaven National Laboratory. Targets were set at 45° to the incident X-ray beam, which was collimated to 7 μm × 7 μm. The beam spread over and excited the volume underlying an area of 10 μm × 7 μm, which was about one-third of the area of the Stardust fragments. We chose for analysis the portion of each grain that gave the highest Fe K_α count rate. In so doing, we may have biased the results toward iron-rich compositions. Element abundances were determined by comparison of fluorescence intensities to those of standards from the National Institute of Standards and Technology.

Optical Microscopy and SEM-EDAX

After nuclear reaction analysis, the three fragments were photographed with a light microscope and coated with carbon in preparation for study with the scanning electron microscope (SEM) at Dartmouth College. Because the fragments presented no flat, polished surface, quantitative elemental analyses were not possible. We were, however, able to image the fragments and take point spectra with the SEM and hence to obtain qualitative information about their compositions. The electron accelerating voltage was 15 keV, the spot size 3 μm^2, and the working distance between sample and electron source 10 mm. Typical count rates were ~1000 counts per second, or 200,000 counts over the 200 s analysis time, with dead times of 15–20%. Typical count rates in the (energy-dispersive) detector were approximately 1000 Hz with dead times of 15–20%. C51 had been potted in epoxy and sectioned. We did not carbon coat this particle and we examined it using the SEM's low-vacuum mode (0.9 torr of water vapor), at a 20 keV accelerating voltage, a spot size of 5 μm^2 and a 10 mm working distance.

RESULTS

IR Spectroscopy

The FTIR spectra from C21 and C23 (Fig. 4) have many of the same features reported by Keller et al. (2006) for other Stardust fragments. They show a strong Si-O stretching feature from 1100–900 cm^{-1}, i.e., in the same range as do spectra for both amorphous silicates and silica aerogel. They

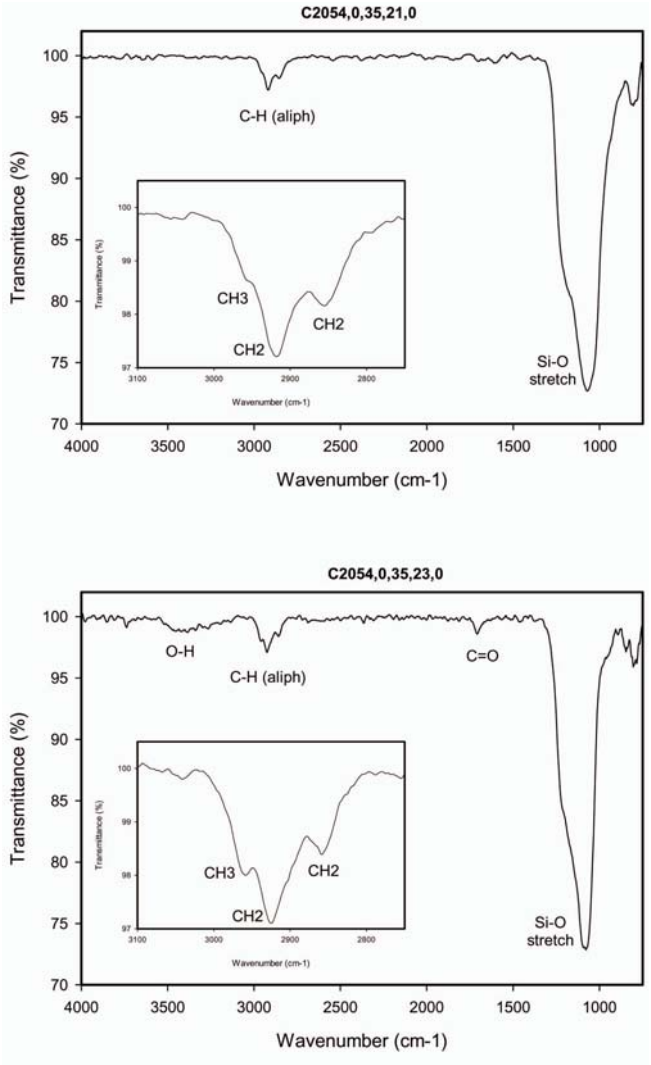

Fig. 4. Infrared spectra of fragments C21 and C23.

also exhibit several absorption features in the C-H stretching region that are consistent with long chain aliphatic hydrocarbons (Fig. 4), namely,

- a strong CH_2 asymmetric stretch at ~2925 cm^{-1};
- a weaker CH_3 asymmetric stretch at ~2960 cm^{-1};
- a CH_2 stretch near 2855 cm^{-1}.

In addition, weak features due to C=O absorption near 1700 cm^{-1} and O-H absorption near 3400 cm^{-1} appear in the spectrum of C23. The O-H vibrational frequency is similar whether O is bonded to C or to Si (e.g., Bellamy 1954). Although the Stardust aerogel contains organic residue from its manufacture, the IR spectrum of this residue differs from that of organic matter from 81P/Wild 2 (see Keller et al. 2006).

SEM Analysis

C21 is approximately 30 μm long by 10 μm wide and comprises subunits 1 μm to 5 μm in size (Fig. 5). The X-ray

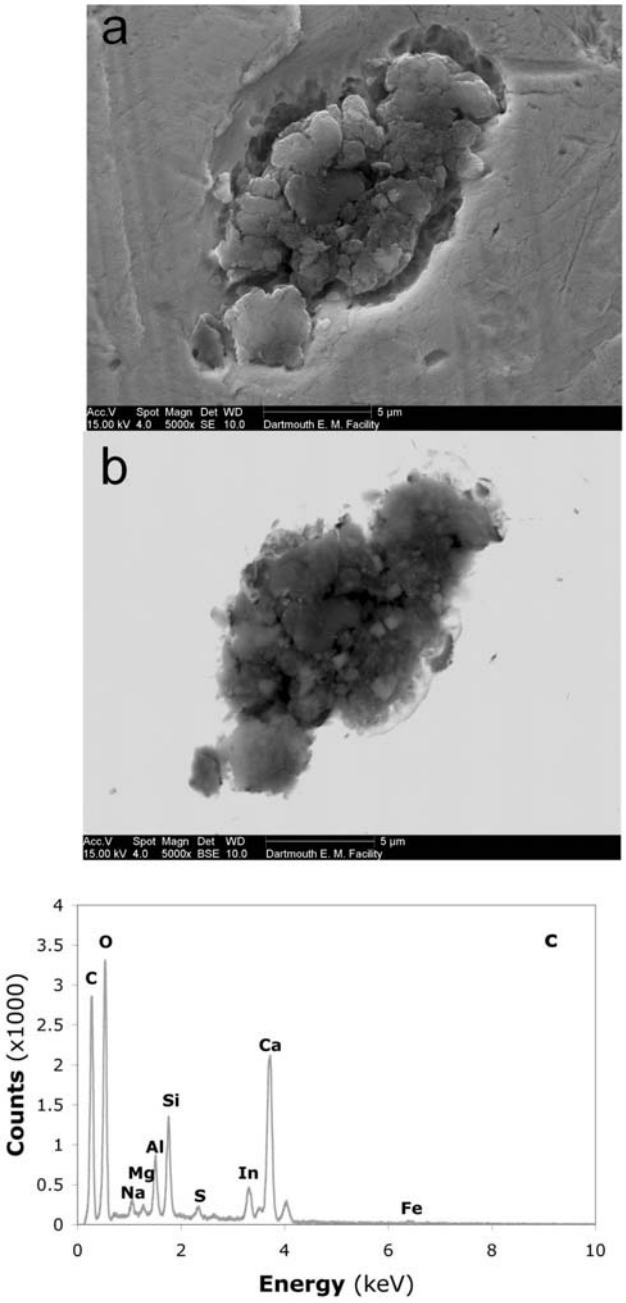

Fig. 5. Fragment C21. a) Secondary electron image. b) Backscatter image. c) EDAX spectrum (counts/1000 versus E (keV).

spectra show O, Si, Al, Ca, Na, Mg, S, and Fe (Fig. 5c), as well as C, at levels well above those attributable to carbon coating. Some Al could have come from the disks used to press the fragments into the indium. As no Al was detectable in the indium foils, however, we discount this possibility. Spot data, as well as element maps, show the presence of small (1 μm × 1 μm) bright grains rich in O and Ca. One such grain was found outside the fragment in the In foil. These grains may be contaminants, although if so, it is odd that they should have concentrated to a greater degree in the fragments than in the surrounding indium. The oxygen map clearly shows the different subunits in the fragment whereas the silicon map shows less detail (element maps not shown). Oxygen and silicon are distributed fairly uniformly over the fragment except for a few places on the periphery where both concentrations are higher.

Fragment C23 has the approximate dimensions 20 μm × 15 μm. In Fig. 6, the fragment looks porous and fluffy much as lint appears to the naked eye. Unlike lint, which is mainly organic, C23 contains Si, O, S, Mg, Fe, and, tellingly, Ni. At high magnification (×20,000) blebs of Fe-S-Ni (Fig. 6d) are seen in the vesicular silicon-rich substrate. From the texture and nature of this assembly, we conclude that this fragment is mainly compressed and heated aerogel.

A portion of fragment C41 was lost during the nuclear reaction analysis. The remaining material measures approximately 5 μm × 5 μm. It contains Si, O, Mg, and lesser amounts of S and Fe (Fig. 7). The indium foils contained blocky crystals composed mainly of Ca and O. We also found rounded particles rich in chlorine and Na-rich needles, which are clearly contaminants.

Particle C51 is shaped like the letter "C", ~20 μm long by 10 μm wide, and composed of a porous material (compressed aerogel) that contains sub-micron bright blebs that consist of iron, nickel, and sulfur in which the Ni/Fe ratio ranges from 0.09 to 0.16 and the S/Fe ratio from 0.14 to 0.30. Eight spots on this fragment were analyzed (Fig. 8). They are compositionally similar and contain Si, O, Mg, Fe, S, Ni, Na, and Al. Chlorine and carbon, from the epoxy, are present in all the spectra. We think this particle, like C23 and C41, is mainly compressed aerogel that contains a melted cometary component.

C, N, O, and Si from Nuclear Reaction Analysis and Fe from Deuteron-Induced X-Ray Fluorescence

In Table 2, we compare the compositions found for NaOCN, KOCN, and $K_3Fe(CN)_6$ with their known compositions. In all three cases, agreement is good, within 10%, for both the fractions of C and N atoms found and for C/N ratios. The fractions of oxygen are higher than expected by about 30% for both NaOCN and KOCN, perhaps because the best available cross section for the $^{16}O(d,p)^{17}O$ reaction was measured at a laboratory angle of 135°, rather than at 170°, the angle relevant for our measurements.

We present the measured atomic percentages of carbon, nitrogen, and oxygen in randomly selected grains from Murchison and Tagish Lake in Table 3. Compared to literature values for Murchison (Table 3), we find higher carbon and nitrogen atomic fractions (×2) than previously reported for grains or for bulk samples. On the other hand, the N/C atomic ratios of ~0.05 agree with literature values within 10% and our measured fraction of atomic oxygen is in

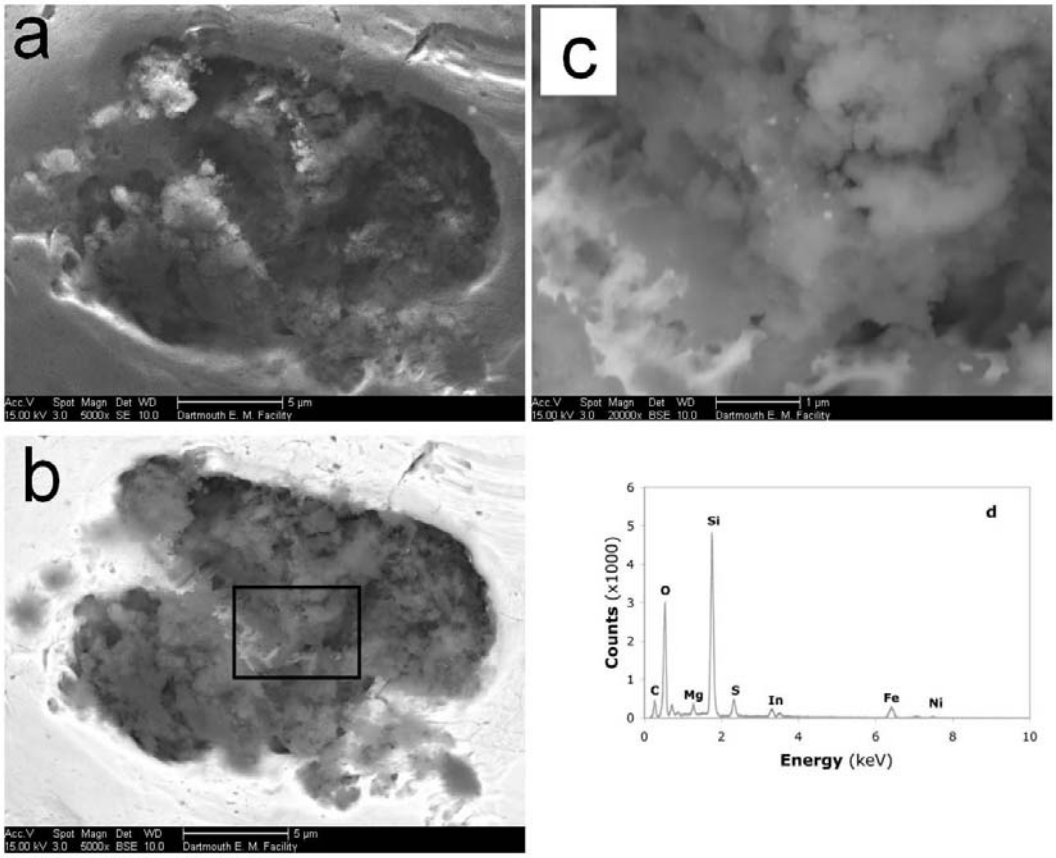

Fig. 6. Fragment C23. a) Secondary electron image. b) Backscatter image. c) Close-up of compressed aerogel in boxed area of (b). d) EDAX spectrum.

Table 2. C, N, and O (atom%) in reagents of known chemical composition.

Sample	C	N	O	N/C	O/C
$K_3Fe(CN)_6$	38.2	41.8		1.10	
Formula	37.5	37.5		1.00	
NaOCN	24.6	26.6	33.0	1.08	1.34
Formula	25.0	25.0	25.0	1.00	1.00
KOCN	24.9	25.5	32.9	1.02	1.32
Formula	25.0	25.0	25.0	1.00	1.00

reasonable agreement with values compiled for bulk samples by Matrajt et al. (2003). Referee Conel Alexander pointed out that carbon and nitrogen are concentrated in the matrix of Murchison so that their measured concentrations will vary with the identity of small particles chosen for study. Our results for carbon and nitrogen in Tagish Lake again exceed published values: the three grains analyzed had ~12 atom% C and 0.45 atom% N, two to three times more than Brown et al. (2000) reported for a bulk sample. The N/C ratios that we measured in Tagish Lake vary considerably, ~40%, but are in the range expected for carbonaceous chondrites.

In Fig. 9 we present the proton spectra for fragments C21 and C23. The spectrum for C41 is very similar to that of C23.

Table 3. C, N, and O (atom%) Murchison and Tagish Lake.

Sample	C	N	O	N/C	O/C
Murchison					
2a	7.23	0.35	55.4	0.048	7.7
4a	6.47	0.35	46.3	0.054	7.2
Grains (1)	4.12	0.18		0.044	
Bulk (1)	2.78	0.13	48.8	0.046	17.5
Tagish Lake					
2a	11.8	0.52		0.044	
2c	12.5	0.50		0.040	
3a	13.4	0.37	55.7	0.028	4.2
Grains[a]	8.0	0.21		0.026	
Bulk[b]	7.9	0.19	44.0	0.024	5.6

[a]Matrajt et al. (2003).
[b]Brown et al. (2000).

Fig. 10 shows elemental maps for C23 created from the nuclear reaction analysis data. The total number of counts per pixel in the carbon map ranged from ~20 at the sample's edge to nearly 1000 toward the interior, where the sample was probably thicker. Over the entire area of fragment C23, carbon and nitrogen occur in an atomic ratio of about 20. In the 4% of the area with the highest observed count rates from carbon and nitrogen, the C/N ratio is nearly the same, 21.

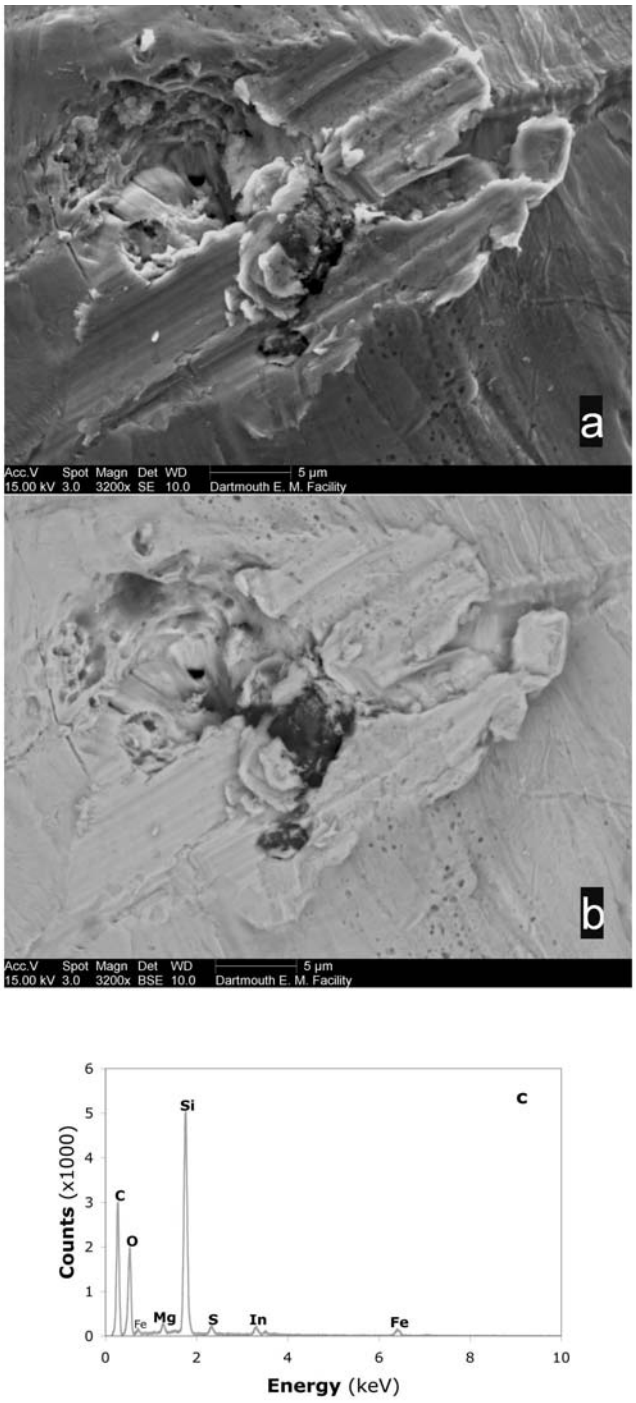

Fig. 7. Fragment C41. a) Secondary electron image. b) Backscatter image. c) EDAX spectrum.

Similar observations apply to fragment C21, although its C/N ratio is different.

To calculate the carbon and nitrogen contents of the Stardust fragments, we need estimates of the amounts contributed by aerogel. In Table 4 we present the results from nuclear reaction analysis of three aerogel samples. For reasons that are not understood, all the carbon contents

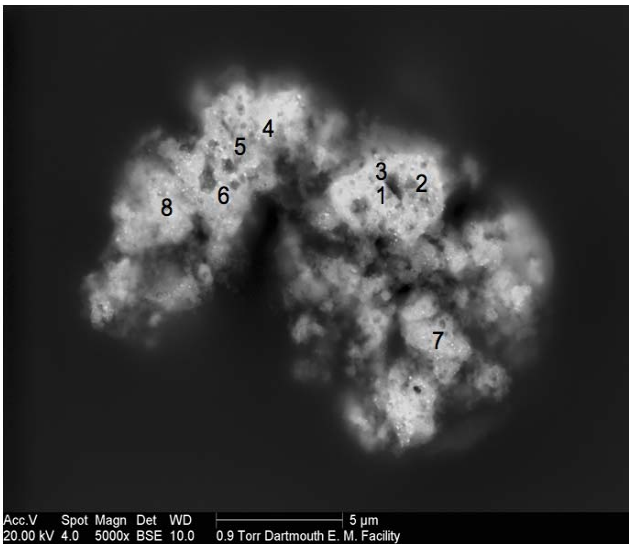

Fig. 8. Fragment C51 showing location of spot analyses.

Table 4. C, N, and O in aerogel samples.

Sample	Si	O	C	N	C/N
			Atom%		
Aerogel 1	28.7	56.1	14.0	1.2	12
Aerogel 3	32.7	65.6	1.6	0.032	50
	32.7	65.9	1.3	0.035	37
Aerogel 4	32.7	64.1	3.1	0.029	107
	32.7	63.8	3.5	0.016	219
Average[a]	**32.7**	**64.9**	**2.4**	**0.031**	**85**
Ref. 1[b]	33.1	66.1	0.82	0.008	~100[c]
			Weight%		
Aerogel 1	42.7	47.5	8.9	0.90	10
Aerogel 3	46.2	52.8	0.97	0.023	43
	46.2	53.0	0.78	0.025	32
Aerogel 4	46.4	51.7	1.9	0.020	92
	46.4	51.5	2.1	0.011	188
Average[a]	**46.3**	**52.3**	**1.4**	**0.020**	**73**
Ref. 1[b]	46.5	53.0	0.5	<0.01	~100[c]

[a]Aerogel 3 and Aerogel 4 (W12TZ); see text.
[b]Tsou et al. (2003) assuming SiO_2 ~99.5 wt%.
[c]G. Cody (personal communication).

exceed the published value of 0.5 wt%. We adopt for our blank the average of two samples of flight-quality material to which nothing else had been done. Excluded, therefore, are the results for Aerogel 1, for which the carbon content of 9 wt% exceeds the published value by a factor of 20, leading us to suspect an artifact or an unrepresentative sample. We note however, the possibility that we have underestimated the blank correction.

In Table 5 we present the results of the nuclear reaction analyses of 3 Stardust fragments. Silicon and oxygen dominate the elemental compositions of fragments C23 and C41. The Si/O atomic ratio of C23 is close to the value of 0.5 expected for silica; the Si/O ratio for C41, is lower, ~0.4,

Table 5. Areas and elemental composition[a] of three fragments recovered from Stardust aerogel.

	C21[b]	C21-bl[c]	C23[b]	C23-bl[c]	C41[b, d]	C41-bl[c]
Area (μm^2)	234		304		252	
C	4.0	4.0	0.66	0.38	0.04	0.003
N	0.078	0.078	0.038	0.035	0.0044	0.0039
C/N	51	51	17	11	10	
O	2.9	2.3	8.0	0.3	1.4	0.31
O[e]		1.6		~0		~0
Mg	<0.07		<0.13		<0.02	
Si	0.30	–	3.8	–	0.53	–
X	1.45	1.45	1.15	1.15	0.14	0.14

[a]Atoms (10^{12}).
[b]Calculated without blank correction.
[c]Corrected for blank by assuming all Si comes from aerogel and the average C and N analyses of aerogel given in Table 4.
[d]Central area of 24 μm^2 only. To compare with C21 and C23, multiply numbers of atoms by ~10.
[e]Calculated with oxygen as measured (previous line) reduced by a factor of 1.3 (see text). X stands for all elements not specifically named above and includes Fe.

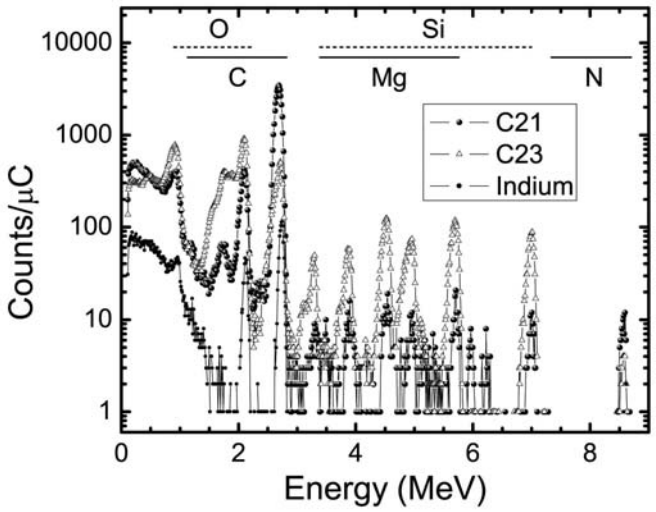

Fig. 9. Proton spectra for fragments C21 and C23 and for an indium foil. The peak for N is free of interferences. Silicon and oxygen produce a minor interference for the peak due to carbon.

which could reflect the presence of extraterrestrial silicates or terrestrial contamination. Alternatively, in the analysis of the cyanates we noted an excess of oxygen of 30%, which could also account for the difference in Si/O ratios. In either case, we conclude from the NRA data that these two fragments contain a sizeable fraction of aerogel, likely melted, an interpretation supported by SEM images and analyses, which show a vesicular Si substrate with submicron FeS-Ni beads.

To correct for the presence of aerogel, we assume that all Si atoms measured in each sample, along with twice that number of oxygen atoms, come from aerogel. These corrections are probably upper limits as some Si may be native to the fragments themselves. Numbers of Si and O atoms corrected for this aerogel blank are shown alongside the uncorrected numbers of atoms in Table 5. The corrections lead to rather small changes in the numbers of C and N atoms in C21, in moderate changes for C23, and large changes for the smallest fragment, C41 (Table 5).

Statistical measurement uncertainties of the elemental ratios are estimated to be 5–10% for C21 and progressively larger for C23 and C41. The calculations of the absolute numbers of atoms assume the samples had uniform density. The results are sensitive to this assumption and consequently have somewhat larger uncertainties than do the elemental ratios. For oxygen, the blank corrections are large and the uncertainties are increased further, and probably dominated by possible systematic errors of 30–40% noted in the discussion of results for chemical reagents.

The C/Si atomic ratios measured by NRA are 13 and 0.1 for C21 and C23, respectively. The FTIR absorbances of the organic features taken relative to the SiO absorbances define a much smaller range, from ~0.04 for OH in C23 to 0.09 for the strong, asymmetric CH_2 stretch. While the raw FTIR absorbances cannot be fully interpreted without standards, the similarity of the ratios of absorbances, A(CH_2 at 2925 cm^{-1})/A(SiO at ~1100 cm^{-1}), is striking. Perhaps C21 contains a large fraction of graphitic carbon (hence the high C/Si ratio from NRA), which would not show up in its FTIR spectrum. Sandford et al. (2006) reported that the fraction of graphitic carbon varies enormously among Stardust fragments.

We could not resolve an iron signal from the spectra of protons produced by nuclear reactions. Quantitation of the deuteron-induced X-ray fluorescence spectra, however, gave the results for iron shown in Table 6. These results refer to the entire samples.

Iron Contents from Synchrotron X-Ray Fluorescence

We present in Figs. 11 and 12 and in Table 6 the results of the SXRF analyses of the three fragments. The spectra show the presence of Ti, Cr, Mn, Fe, Ni, and Zn. We carried out the SXRF analyses in such a way as to optimize the precision of the elemental ratios in the shortest possible time.

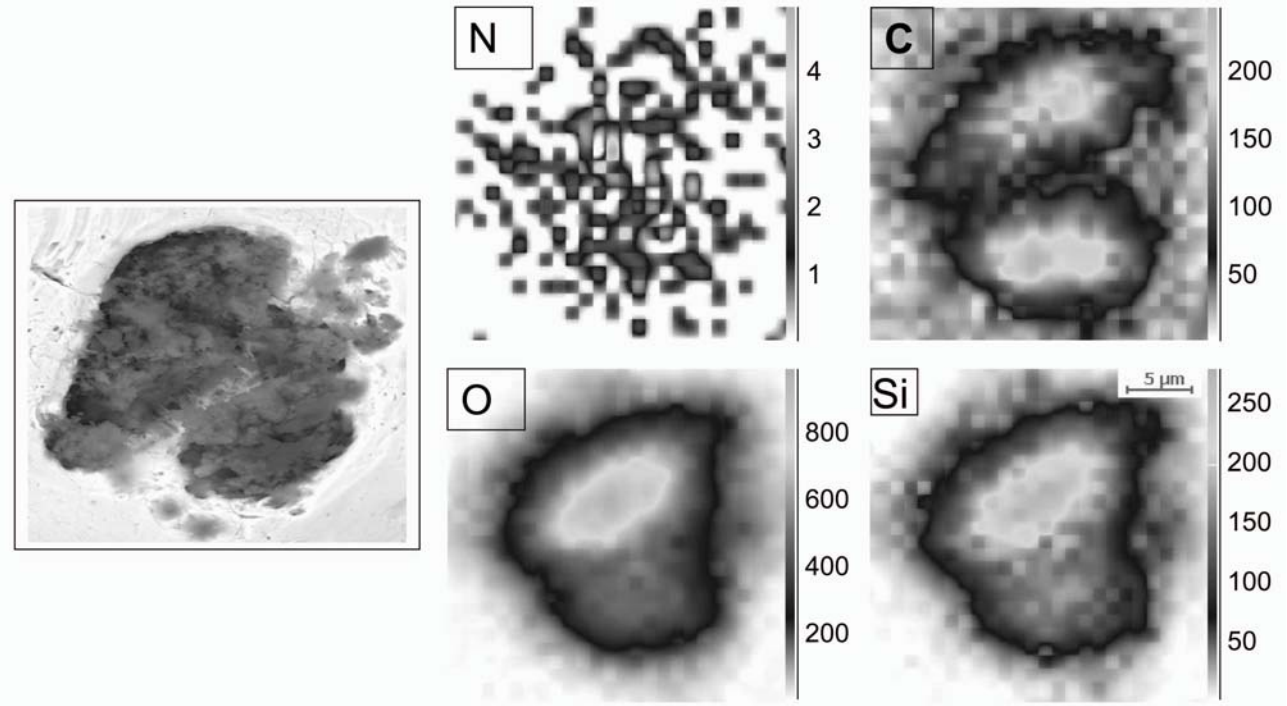

Fig. 10. Backscatter image and elemental maps of N, O, C, and Si from nuclear reaction analysis of fragment C23.

These results also give the masses or numbers of atoms present, but with precision lower than the SXRF method could achieve with a larger X-ray spot size and a longer analysis time. We estimated a blank correction for aerogel for each fragment by assuming the elemental ratios, E/Si, measured by Tsou et al. (2003) and the Si contents measured by nuclear reaction analysis (Table 5), that is, by assuming all of the Si was from the aerogel. Even with this assumption, the calculated blanks were negligible for all elements other than oxygen and silicon. It should be understood, however, that the composition of the material that adheres to the Stardust fragments might differ from that of unaltered aerogel.

Two independent SXRF analyses of C21 carried out at different times agree well for the six elements analyzed, to within ±10%. Figure 12 shows the elemental ratios to iron divided by the same ratios in CI chondrites (i.e., "CI normalized ratios"). They scatter appreciably as Flynn et al. (2006) reported for a much larger number of fragments. In general, the individual Cr/Fe, Mn/Fe, and Ni/Fe ratios lie within a factor of 10 or so of CI values, while Ti is enriched in C21 and Zn in C23 and C41. By all indications, the enrichments reflect the composition of extraterrestrial matter. Still, it is worrisome that aerogel has high Ti/Fe and Zn/Fe ratios.

We can compare directly the numbers of Fe atoms in the samples determined by SXRF (Table 6) and deuteron-induced X-ray fluorescence. The raw SXRF results are smaller by factors of 15, 16, and 26 for C21, C23, and C41, respectively. As noted above, the SXRF beam spot was smaller than the samples, nominally by factors of 3.3, 4.3, and 3.6. The exact factor depends on the distribution of mass in each fragment. Overall, therefore, the iron contents measured by the two techniques differ by at least a factor of 4 for iron. Further work is needed to reconcile this difference. It seems clear however, that iron is less abundant than carbon in these fragments.

Element Ratios from SXRF

We calculate mean, CI-normalized, elemental ratios of the three Stardust fragments from the SXRF data only in two ways: as geometric means of the ratios for as many fragments as we have data; and from the total masses found in all three fragments (Table 7). The latter include null values and may be smaller than the former. For example, the "total" Ti/Fe ratio includes null values for Ti in C23 and C41. With either method of calculation, Mn/Fe, Cr/Fe, and Ni/Fe ratios agree with CI values to within a factor of two or so. Flynn et al. (2006) calculated elemental ratios for 23 whole tracks and reported that most of them matched CI values to within 50%.

DISCUSSION

Cometary Origin

Several observations indicate that the fragments come from Wild 2. First, C23, C41, and C51 are embedded in compressed or partially melted aerogel. Second, the SEM results for these three fragments show the presence of finely dispersed, sub-micron beads of Fe-Ni-S probably originally a

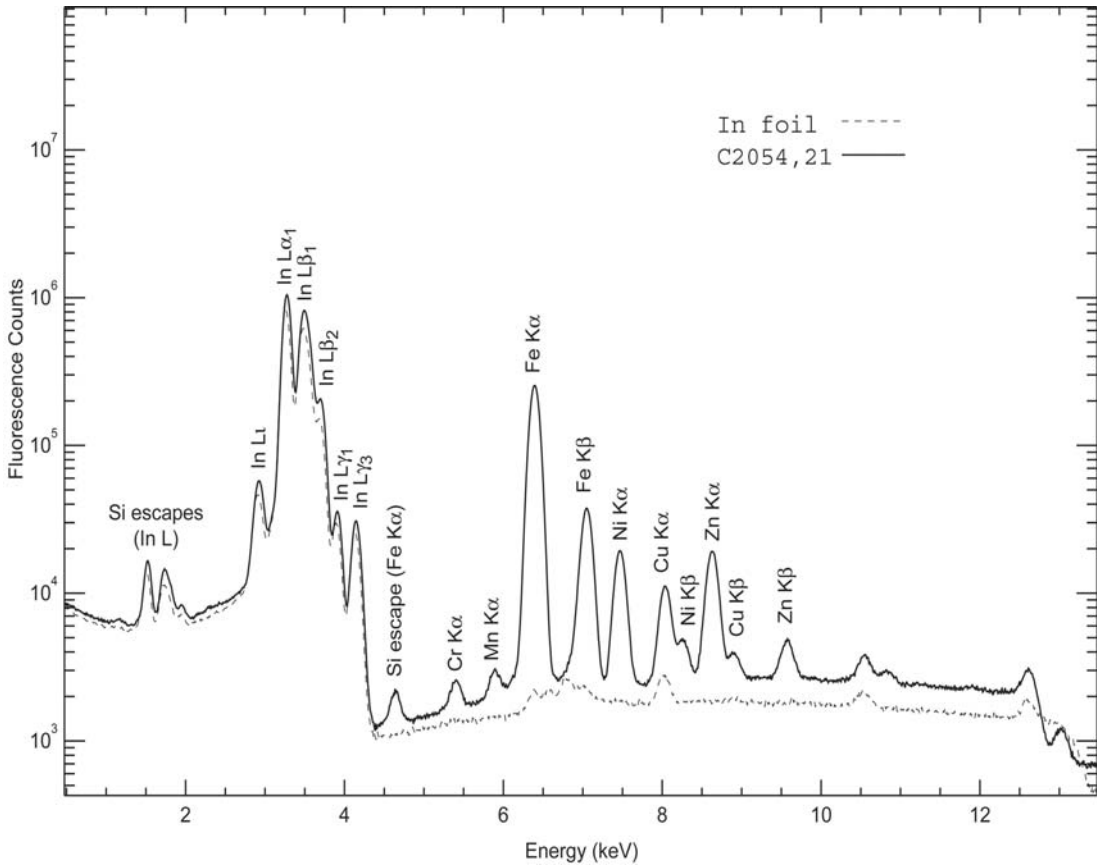

Fig. 11. SXRF spectra for fragment C21 and for indium. Counts from titanium (4.5 keV, not labeled) occur in the low energy shoulder of the Fe K_α–Si escape peak (4.7 keV). We extracted the counts due to titanium by standard fitting procedures.

Table 6. Fe contents (10^9 atoms) and elemental ratios × 1000 (atomic) of Stardust fragments and aerogel.

	Fe[a]	Fe[b]	Ti/Fe	Cr/Fe	Mn/Fe	Ni/Fe	Zn/Fe
C21	3.1		130	12.4	17.4	6.1	216
C21	2.9		104	–	14.5	6.8	185
C21 avg	3.0	46	117	6.3	11.7	6.4	201
C23	11.6	190	–	17.9	11.7	205	–
C41[a]	6.6	170	–	8.2	6.4	56	33
CI			2.8	15.6	10.7	58	1.5
Aerogel[c]			82	21	17	49	720

[a]SXRF. Beam was smaller than the sample by a factor of about 4; no adjustment has been made for this effect.
[b]Deuteron-induced X-ray fluorescence. Beam covered the entire sample.
[c]Tsou et al. (2003).

nickel-bearing Fe sulfide. Third, the three fragments analyzed by SXRF (C21, C23, and C41) contain measurable concentrations of nickel with Cr/Fe, Mn/Fe, and Ni/Fe ratios at or near-CI values and quite distinct from the ratios in most naturally occurring terrestrial materials, although not from aerogel itself. Fragment C21 is morphologically unusual and needs more study. Its high C content, Ni/Fe ratio, and position within the aerogel all suggest that it is extraterrestrial. Most Wild 2 fragments described to date are either anhydrous silicates or compressed aerogel that contains cometary material. Fragments C23 and C41 are examples of the latter (Zolensky et al. 2006).

Masses and Densities

We estimate total fragment masses, including aerogel, by assuming that: 1) the elements listed in Table 5 account for virtually all of the atoms present in the samples; 2) X comprises Mg, Al, S, Ca, and Fe in CI chondritic proportions and therefore has a mean molar mass of 37.0 g/mol; and 3) aerogel contributions to all elements other than Si and O are negligible. The calculated fragment masses are then as follows: C21, 0.26 ng; C23, 0.48 ng; C41, 0.07 ng. These results are not very sensitive to the molar mass assumed for X.

To constrain the densities, ρ, of the fragments, we need

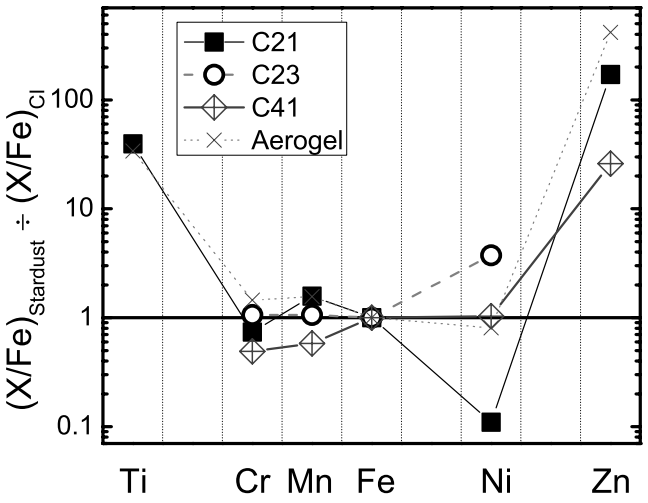

Fig. 12. Elemental ratios to iron normalized to the corresponding ratios in CI chondrites for three Stardust fragments and for aerogel.

Table 7. Combined elemental ratios to iron normalized to CI chondrites.

Ratio	Geom. mean	Total
Ti/Fe	36	5.0
Cr/Fe	0.73	0.84
Mn/Fe	0.96	10.97
Ni/Fe	10.77	2.4
Zn/Fe	64	31

their volumes. The areas of the fragments were measured by microscopy (Table 2) but their thicknesses are unknown. To calculate maximum likely densities we model the fragments as uniform flat plates with a thickness of 1 μm. Any smaller value would have led to SEM indium backgrounds much larger than those observed. With a thickness of 1 μm we find ρ = 1.0 g/cm^3 for C21; 1.6 g/cm^3 for C23; and 2.9 g/cm^3 for C41. Within the uncertainties, these values are consistent with upper bounds set by plausible components of the fragments, namely quartz/compacted aerogel (2.6 g/cm^3), graphitic organic material (2.25 g/cm^3), and CI meteorites (2.3 g/cm^3). If instead, we model the fragments as spheres with radii taken as $\sqrt{\text{Area}/\pi}$, we obtain densities (g/cm^3) of 0.1, 0.1, and 0.8 for C21, C23, and C41, respectively.

Weight Percentages

The weight percentages of carbon and nitrogen in the three fragments as received, i.e., without correcting for the presence of aerogel are as follows: C21, 30 and 0.7; C23, 2.8 and 0.2; C41, 1.2 and 0.14. By coincidence, the carbon and nitrogen concentrations calculated for C23 and C41 resemble those of CM chondrites, 2.2 wt% C, and 0.15 wt%. With the assumption that all Si comes from aerogel, the carbon and nitrogen concentrations become: for C21, 37 and 0.85; and for C23, 9.5 and 1.0. For C41, we obtain nominal values of 0.7 and 1, but the uncertainties are very large. The weight percentages found for C21 and C23 are large compared to those in carbonaceous meteorites, probably in part because we have effectively set the silicon content to zero.

Oxygen/Carbon Ratios

After correction for aerogel contamination, the O/C atomic ratio in C21 is ~0.6 (Table 5). This result is in the range of XANES determinations of O/C ratios in other Stardust fragments (0.2 to 0.6; Sandford et al. 2006) and considerably higher than the ratio of 0.14 typical of the organic phases of carbonaceous chondrites (Pizzarrello et al. 2006). The identity of oxygen's partner is unclear from our data. The IR spectrum of C21 appears to exclude both hydroxyl groups—and hence water—and carbonyl groups. The number of Fe atoms measured by deuteron-induced XRF is too small by a factor of 10 to bind with all the oxygen (Table 6) and the proton spectrum sets an upper limit on Mg of ~1 atom%. By elimination, it would seem that the oxygen is bound as aromatic heteroatoms as suggested by Sandford et al. (2006).

For fragments C23 and C41, the numbers of oxygen atoms remaining after the correction for aerogel are positive, but do not differ significantly from zero within the 1σ uncertainties of 30% set by the oxygen measurements. Fragment C23 does show the presence of O-H and C=O features in its IR spectrum (Fig. 4). In this case, however, we cannot tell whether the O-H is bound to Si, C, or perhaps even H.

Carbon/Nitrogen Ratios

The most primitive extraterrestrial materials appear to have the highest carbon and nitrogen contents and the lowest C/N ratios. The C/N ratios increase from 4 in the Sun, to ~10 in CI chondrites, IDPs, and Halley dust and ice; to values greater than 50 in the CO and CV chondrites, which have higher metamorphic temperatures (Table 8). Kissel et al. (2004) reported high nitrogen contents in grains from comet 81P/Wild 2 analyzed remotely, but did not specify C/N ratios. Overall, the trend in C/N ratios presumably reflects the higher volatility of N-rich compounds of low molecular weight and the relatively low thermodynamic stability of N-bearing solids under nebular and asteroidal conditions.

The C/N atomic ratios are 51 for C21, 11–17 for C23, and <10 for C41, values more or less within the meteoritic range. It is unclear how faithfully these measured values represent the C/N ratios of the original impactors. Although aerogel may have helped to insulate fragments C23 and C41 as they decelerated, heating probably altered the organic matter to some degree. Direct studies of the regions surrounding the tracks show that organic material is widely dispersed (see Sandford et al. 2006). Based on these observations and the general trend toward higher C/N ratios noted above, we infer

Table 8. C/N ratios (atomic) of extraterrestrial materials.

Sample	C/N	Ref.
Stardust fragments		
C41	10	a
C23 whole	17	a
C23 center	21	a
C21 whole	51	a
C21 center	45	a
Sun	4	b
Halley dust & ice	10.6	c
IDPs	10–50	d, e
CI	12.6	f
Micrometeorites	15–80	e
CM	16.9	f
Halley dust	19.4	c
Comets	20	g
Murchison	21.4	f
Tagish Lake	41.7	f
CO	57.0	f
CV	77.3	f
Coal macerals	50–100	h

[a]This work without correction for aerogel blank. For corrected values, see Table 5.
[b]Asplund et al. (2005).
[c]Jessberger and Kissel (1991).
[d]Keller et al. (1995).
[e]Matrajt et al. 2003.
[f]Lodders and Fegley (1998).
[g]Calculated from Table 1 of Bockelée-Morvan et al. (2004).
[h]Mastalerz and Gurba (2001).

that our measured C/N ratios represent upper limits for the original C/N ratios of the organic material in the impactors—that is, that the fragments may have lost N preferentially on capture. How well the impactors represent the bulk comet is a separate question. Analyses of larger fractions of the particle tracks for carbon and nitrogen would be desirable to check for evidence of nitrogen not retained by fragments, as would studies of the behavior of carbon rich materials during high-velocity impacts with aerogel.

Vaporization of Stardust Particles?

Brownlee et al. (2006) argued that the large volumes of bulbous tracks in aerogel owe primarily to the dispersion of fine-grained particles that remained intact, but acknowledged the possibility that some vaporization of volatile materials took place. Gaseous water is by far the most common volatile observed remotely in the comae of many comets (Bockelée-Morvan et al. 2004; Brownlee 2004), Wild 2 among them (Farnham and Schleicher 2005). Lellouch et al. (1998) reported the presence of $H_2O(s)$ in comet Hale-Bopp, at a distance of 2.9 AU from the Sun. These observations notwithstanding, Kissel et al. (2004) found no water in the mass spectra collected for 29 particles during flyby of Wild 2. Whether any water or other ices, perhaps mantled by protective layers, survived passage from Wild 2 to the Stardust collector without subliming is not known. But even if ice did not reach the collector, the composition of our fragments and the results of Sandford et al. (2006) show that some material rich in carbon, nitrogen, and oxygen materials did so.

How much vaporization might we expect from the impact of such materials? F. Hörz performed experiments in which grains of Illinois coal were fired at ~6 km/s into aerogel. The impacts produced large tracks but no detectable terminal particles, demonstrating that the coal vaporized during capture. Kissel et al. (2004) concluded that oxygen-poor, nitrogen-rich compounds, and in particular "nitriles and polymerization products of hydrocyanic acid," were the likely constituents of the particles that they analyzed during the encounter of Stardust with Wild 2. The nature of their instrument, the Cometary and Interstellar Dust Analyzer (CIDA), allowed Kissel and coworkers to detect only material that vaporized on striking the detector plate. They were therefore careful to note that they may have analyzed only a thin layer of organic matter coating inorganic grains. The C/N ratios that we measured for fragments are considerably larger than for polymers of HCN or nitriles of low molecular weight. Accordingly, we suggest that the higher C/N ratios of the fragments reflect the loss through vaporization of molecules with lower molar masses and C/N ratios.

To estimate the mass of vaporized impactor required to make a turnip-shaped track, we assume that the bulbous portion formed when organic matter vaporized and expanded adiabatically. Table 9 shows the results of three approaches. The first one assumes a reversible adiabatic expansion of an ideal gas; the second one assumes an adiabatic expansion against a constant pressure equal to the crushing strength of the aerogel (see below). The third is based on the work of Domínguez et al. (2004), who calculated the volume generated by the deceleration of solid (not gaseous) cometary matter only.

We assume that the gas consisted of a mixture of ethane, hydrogen cyanide, and CH_3OH in the molar ratio 1:1:1. At very high initial temperatures, the molecules might dissociate completely, in which case we would expect $C_p/C_V = \gamma \sim 5/3$ and $C_V \sim 3/2R$, where C is the heat capacity at constant pressure (p) or volume (V). On the other hand, for the (undissociated) molecules, γ is on the order of 1.1–1.2 J mol^{-1} K^{-1} for temperatures from ~500 K to ~2400K and the experimental values of Cv are closer to 12R. We consider these ranges—$3/2R < C_V = < 12R$ and $5/3 > \gamma > 1.2$—of possible values below.

The final volume of the gas is taken as that of the bulbous portion of the track. Expansion presumably stopped when the pressure of the gas equaled the crushing strength of the aerogel. From the relation given by Domínguez et al. (2004, equation 18) and assuming an uncompressed aerogel density of 7 mg/cm^3 (A. Westphal, personal communication), we calculate the external/final pressure to be 1.47 kPa. Next, we assume that the initial volume of the gas is given by the mass

Table 9. Mass required to produce a spherical track with a volume of 33 mm^3.[a]

	V_2/V_1	m/V_2	C_V	γ	m
Reversible adiabatic expansion	$\left(\frac{p_1}{p_2}\right)^{1/\gamma}$	$\left(\frac{p_2}{p_1}\right)^{1/\gamma}\rho_g$	3/2R	5/3	1653
			12R	1.2	38
Adiabatic expansion at constant external pressure	$\frac{C_v}{R}\frac{p_1}{p_2}$	$\rho_g\frac{R}{C_v}\frac{p_2}{p_1}$	3/2R	5/3	1.7
			12R	1.2	0.22
Domínguez et al. (2004)	$4\left(\frac{\rho_g}{\rho_o}\right)^{1/2}\left(\frac{p_1}{p_2}\right)^{1/2}$	$\frac{1}{4}(\rho_g\rho_o)^{1/2}\left(\frac{p_1}{p_2}\right)^{1/2}$			776

[a]V_1 is the initial volume of the cometary solid; V_2 is the volume of the track; m is the mass of cometary material assumed to have vaporized in the adiabatic expansion (but not in the calculation of Domínguez et al. (2004), where no vapor forms, and where m is the mass of the solid). C_V is the heat capacity of the gas at constant volume; R is the gas constant, 8.314 J mol^{-1} K^{-1}; and γ is the ratio C_p/C_V, where C_p is the heat capacity at constant pressure. p_1 is the initial pressure that the cometary mass exerts on the aerogel; p_2 is the crushing strength of the aerogel. ρ_g is the density of the solid cometary material and ρ_o the density of the aerogel. The formula for V_2/V_1 is derived from Equations 4 and 28 of Domínguez et al. (2004), with the additional substitution that $p_1 = 1/2\ \rho_g\ v_o^2$, where v_o is the velocity of the cometary particle. This pressure is nominal in the context of the model of Domínguez et al. (2004) and should not be interpreted as a physical pressure. The last column gives the value of m, the mass required (ng) to produce a track with a volume of 33 mm^3.

of volatile material, m, divided by its density when solid, ρ_g, $V_i = m/\rho_g$ We adopt a particle density, ρ_g, of 0.8 g/cm^3, consistent with results obtained above and estimate the initial pressure from the relation $p_1 = 1/2\ \rho_g\ v^2 = 1.5 \times 10^7$ kPa, where V_o is the encounter velocity of the cometary particle, 6.1 km/s.

As expected, the mass, m, required to make a track of a given volume is considerably smaller in the case of the expansion against constant, relatively low pressure, which seems the more realistic model (Table 9). In this model, reduction of the initial pressure by a factor of 10 raises the required mass by the same factor. A portion of the track volume may derive from displacement of aerogel by solid cometary matter as described by Domínguez et al. (2004), rather than by vaporized cometary matter. As the calculated mass of volatile material scales as the track volume, V_2, reduction of V_2 by, say, a factor of five to allow for the volume attributable to the non-volatile component reduces m by the same factor. In sum, we find that vaporization of relatively small masses of volatile material could make a substantial contribution to the observed volume of a track.

We now turn to the estimation of the mass fractions of carbon and nitrogen in the incoming particles. The fragments that we analyzed, C21 and C23 were selected partly for their unusually large sizes and masses, estimated above as 0.26 and 0.48 ng, respectively, including aerogel. If track 35 contains another 30, presumably smaller, fragments with an average mass of 0.074 ng (1/5th the average for C21 and C23), then the total fragment mass in track 35 would sum to 3 ng, a value comparable to the masses estimated for volatilized material, but apparently much less than the mass of unvaporized solid required to generate the volume observed (Table 9). Reductions of the Stardust fragment masses to allow for the presence of aerogel and the presence of non-volatile components would seem only to strengthen this inference. Our preferred conclusion is that the fragments analyzed retain a small fraction of the carbon and nitrogen present when the particles entered the aerogel. Whether the carbon and nitrogen escaped during the long voyage home under vacuum or were converted to more refractory, stationary, and perhaps detectable forms remains to be seen. IR transmission measurements (see Sandford et al. 2006) indicate that the aerogel retains dispersed organic matter.

CONCLUSIONS

Three Stardust fragments identified as carbon-rich by their IR spectra and/or dark appearance under the microscope contain approximately chondritic proportions of the elements Mn, Cr, and Ni, a finding consistent with the results for 23 whole tracks and with an extraterrestrial origin (Flynn et al. 2006). Two of the fragments contain 10 weight percent or more of carbon and 10× to 50× less nitrogen. The amounts of C and N present in the third fragment, C41, are highly uncertain because of the presence of aerogel. Although commingling of the cometary particles with aerogel makes the exact percentages of carbon and nitrogen difficult to determine, the original percentages—i.e., the ones prior to impact—seem to be as large as or larger than those found in carbonaceous chondrites. The carbon and nitrogen contents of C21 and C23 appear to be similar to some of those described by Fomenovka et al. (1994) for particles from Halley. The heterogeneity of the particles implies that analyses of numerous fragments and additional blank studies will be needed to reconstruct abundances in the Wild-2 particles prior to capture.

Measured C/N atomic ratios span the range set by IDPs, Halley dust and ice, and CI chondrites at the low end (~10), and by CO and CV chondrites at the high end (~60). To the degree that the Stardust collector encountered particles with compositions similar to that of pristine Wild 2 (i.e., material that had not experienced sublimation losses), we infer that deceleration in aerogel likely caused larger losses of nitrogen than of carbon in some fragments, thereby increasing the measured C/N ratios in the residual material. An associated

expansion of gas may have contributed measurably to the observed volumes of the tracks. If so, it would be interesting to scan entire track volumes and their immediate surroundings for carbon and nitrogen released from the particles. Assuming that aerogel retained any vaporized carbon and nitrogen from the comet, the presence of carbon and nitrogen in the aerogel capture medium could hamper such analyses. In any case, laboratory studies of well-characterized materials striking aerogel at high velocities could help in understanding how bulbous tracks formed as could additional analyses of a representative suite of fragments.

Acknowledgments–We thank Keiko Messenger, Mike Zolensky, Christopher Snead, and Andrew Westphal for their efforts to select and separate the samples analyzed; Didier Guillier, François Saillant, Pascal L'Hénoret, Laurent Daudin, and the staff of the Laboratoire Pierre Süe for assistance with the carbon and nitrogen measurements; and Don Burnett, George Cody, G. Domínguez, Tony Farnham, Fred Hörz, and reviewers Conel Alexander and anonymous for useful comments. We thank Ralph Knowles and the FEI Company for loan of a gaseous analytical detector.

This work was supported in part by NASA grants NAQG5-11719 (GFH), NNG06GG13G (GJF). Portions of this work were performed at Beam line X26A, National Synchrotron Light Source (NSLS), Brookhaven National Laboratory. X26A is supported by the Department of Energy (DOE) Geosciences (DE-FG02-92ER14244 to the University of Chicago—CARS) and DOE—Office of Biological and Environmental Research, Environmental Remediation Sciences Division (DE-FC09-96-SR18546 to the University of Georgia). Use of the NSLS was supported by DOE under contract no. DE-AC02-98CH10886.

Editorial Handling—Dr. Scott Sandford

REFERENCES

A'Hearn M. F., Millis R. L., Schleicher D. G., and Osip D. J. 1995. The ensemble properties of comets: Results from narrow band photometry of 85 comets, 1976–1992. *Icarus* 118:223–270.

Asplund M., Grevesse N., and Sauval A. J. 2005. The solar chemical composition. In: *Cosmic abundances as records of stellar evolution and nucleosynthesis in honor of David L. Lambert*, edited by Barnes T. G. III and Bash. F. N. ASP Conference Series vol. 336. pp. 25–38.

Bellamy L. J. 1954. *The infra-red spectra of complex molecules*. New York: John Wiley & Sons. 425 p.

Bockelée-Morvan D., Crovisier J., Mumma M. J., and Weaver H. A. 2004. The composition of cometary volatiles. In: *Comets II* edited by Festou M. C., Keller H. U., and Weaver H. A. Tucson, Arizona: The University of Arizona Press. pp. 391–423.

Brown P. G., Hildebrand A. R., Zolensky M. E., Grady M., Clayton R. N., Mayeda T. K., Tagliaferri E., Spalding R., MacRae N. D., Hoffman E. L., Mittlefehldt D. W., Wacker J. F., Bird J. A., Campbell M. D., Carpenter R., Gingerich H., Glatiotis M., Greiner E., Mazur M. J., McCausland P. J. A., Plotkin H., and Mazur T. R. 2000. The fall, recovery, orbit, and composition of the Tagish Lake meteorite: A new type of carbonaceous chondrite. *Science* 290:320–325.

Brownlee D. E. 2004. Comets. In: *Meteorites, comets, and planets*, edited by Davis A. M. Treatise on Geochemistry, vol. 1. Amsterdam: Elsevier. pp. 663–688.

Brownlee D., Tsou P., Aléon J., Alexander C. M. O'D., Araki T., Bajt S., Baratta A., Bastien R., Bland P., Bleuet P., Borg J., Bradley J. P., Brearley A., Brenker F., Brennan S., Bridges J. C., Browning N. D., Brucato J. R., Bullock E., Burchett M. J., Busemann H., Butterworth A., Chaussidon M., Cheuvront A., Chi M., Cintala M. J., Clark B. C., Clemett S. J., Cody G., Colangeli L., Cooper G., Cordler P., Daghlian C., Dai Z., D'Hendecourt L., Djouadi Z., Domínguez G., Duxbury T., Dworkin J. P., Ebel D. S., Economou T. E., Fakra S., Fallon S., Fairey S. A. J., Ferrini G., Ferroir T., Fleckenstein H., Floss C., Flynn G., Franchi I. A., Fries M., Gainsforth Z., Gallien J.-P., Genge M., Gilles M. K., Gillet P., Gilmour J., Glavin D. P., Gounelle M., Grady M. M., Graham G. A., Grant P. G., Green S. F., Grossemy F., Grossman L., Grossman J. N., Guan Y., Hagiya K., Harvey R., Heck P., Herzog G. F., Hoppe P., Hörz F., Huth J., Hutcheon I. D., Ignatyev K., Ishii H., Ito M., Jacob D., Jacobsen C., Jacobsen S., Jones S., Joswiak D., Jurewicz A., Kearsley A. T., Keller L. P., Khodja H., Kilcoyne A. L. D. Kissel J., Krot A., Langenhorst F., Lanzirotti A., Le L., Leshin L. A., Leitner J., Lemette L., Leroux H., Liu M.-C., Luening K., Lyon I., MacPherson G., Marcus M. A., Marhas K., Marty B., Matrajt G., McKeegan K., Meibom A., Mennella V., Mesenger K., Messenger S., Mikouchi T., Mostefapio S., Nakamura T., Nakano T., Papanastassiou D. A., Palma R., Palumbo M. E., Pepin R. O., Perkins D., Perronnet M., Pianetta P., Rao W., Rietmeijer F. J. M., Robert F., Rost D., Rotundi A., Ryan R., Sandford S. A., Schwandt C. S., See T. H., Schlutter D., Sheffield-Parker J., Simionovici A., Simon S., Sitnitsky I., Snead C. J., Spencer M. K., Stadermann F. J., Steele A., Stephan T., Stroud R., Susini J., Sutton S. R., Suzuki V., Taheri M., Taylor S., Teslich N., Tomeokoa K., Tomioka N., Toppani A., Trigo-Rodríguez J. M., Troadec D., Tsuchiyama A., Tuzzolino A. J., Tyliszczak T., Uesugi K., Velbel M., Vellenga J., Vicenzi E., Vincze L., Warren J., Weber I., Weisberg M., Westphal A. J., Wirick S., Woioden D., Wopenka B., Wozniakiewicz P., Wright I., Yabuta H., Yano H., Young E. D., Zare R. N., Zega T., Ziegler K., Zimmerman L., Zinner E., and Zolensky M. 2006. Comet 81P/Wild 2 under a microscope. *Science* 314:1711–1716.

Chyba C. F. and Sagan C. 1992. Endogenous production, exogenous delivery and impact-shock synthesis of organic molecules: An inventory for the origins of life. *Nature* 355:125–132.

Dauphas N. 2003. The origin of the terrestrial atmosphere: Early fractionation and cometary accretion (abstract #1813). 34th Lunar and Planetary Science Conference. CD-ROM.

Domínguez G., Westphal A. J., Jones S. M., and Phillips M. L. F. 2004. Energy loss and impact cratering in aerogels: Theory and experiment. *Icarus* 172:613–624.

Farnham T. L. and Schleicher D. G. 2005. Physical and compositional studies of comet 81P/Wild 2 at multiple apparitions. *Icarus* 173:533–558.

Flynn G. J., Bleuet P., Borg J., Bradley J. P., Brenker F. E., Brennan S., Bridges J., Brownlee D. E., Bullock E. S., Burghammer M., Clark B. C., Dai Z. R., Daghlian C. P., Djouadi Z., Fakra S., Ferroir T., Floss C., Franchi I. A., Gainsforth Z., Gallien J.-P., Gillet P., Grant P. G., Graham G. A., Green S. F., Grossemy F., Heck P., Herzog G. F., Hoppe P., Hörz F., Huth J., Ignatyev K., Ishii H. A., Janssens K., Joswiak D., Kearsley A. T., Khodja H., Lanzirotti A., Leitner I., Lemelle L., Leroux H., Luening K., MacPherson G. J.,

Marhas K. K., Marcus M. A., Matrajt G., Nakamura T., Nakamura-Messneger K., Nakano T., Newville M., Papanastassiou D. A., Pianetta P., Rao W., Riekel C., Rietmeijer F. J. M., Rost D., Schwandt C. S., See T. H., Sheffield-Parker J., Simionovici A., Sitnitsky I., Snead C. J., Stadermann F. J., Stephan T., Stroud R. M., Susini J., Suzuki Y., Sutton S. R., Taylor S., Teslich N., Troadec D., Tsou P., Tsuchiyama A., Uesugi K., Vekemans B., Vicenzi E., Vincze L., Westphal A. J., Wozniakiewicz P., Zinner E., and Zolensky M. E. 2006. Elemental composition of comet 81P/Wild 2 samples collected by Stardust. *Science* 314:1731–1734.

Fomenkova M. N., Chang S., and Mukhin L. M. 1994 Carbonaceous components in the comet Halley dust. *Geochimica et Cosmochimica Acta* 58:4503–4512.

Gallien J.-P. Orberger B., Daudin L., Pinti D. L., and Pasava J. 2004. Nitrogen in biogenic and abiogenic minerals from Paleozoic black shales: an NRA study. *Nuclear Instruments and Methods in Physical Research B* 217:113–122.

Herzog G. F., Hanson A. L., Jones K. W., and Smith J. V. 1985. Determination of ^{14}N in iron meteorites by nuclear reaction analysis. *Eos* 66:1145.

Herzog G. F., Gallien J.-P., Khodja, H., Flynn G. J., and Taylor S. 2006. Preparation for cometary sample return: nuclear microprobe analysis of carbon and nitrogen in NaOCN, KOCN, $K_3Fe(CN)_6$, Tagish Lake, Murchison, and two cosmic spherules (abstract 1694). 37th Lunar and Planetary Science Conference. CD-ROM.

Hörz F., Bastien R., Borg J., Bradley J. P., Bridges J. C., Brownlee D. E., Burchell M. J., Chi M., Cintala M. J., Dai Z. R., Djouadi Z., Domínguez G., Economou T. E., Fairey S. A., Floss C., Franchi I. A., Graham G. A., Green S. F., Heck P., Hoppe P., Huth J., Ishii H., Kearsley A. F., Kissel J., Leitner J., Leroux H., Marhas K., Messenger K., Schwandt C. S., See T. H., Snead C., Stadermann F. J., Stephan T., Stroud R., Teslich N., Trigo-Rodríguez J. M., Tuzzolino A. J. Troadec D., Tsou P., Warren J., Westphal A., Wozniakiewicz P., Wright I., and Zinner E. 2006. Impact features on Stardust: Implications for comet 81P/Wild 2 dust. *Science* 314:1716–1719.

Jessberger E. K. and Kissel J. 1991. Chemical properties of cometary dust and a note on carbon isotopes. In: *Comets in the post-Halley era*, edited by Newburn R., Neugebauer M., and Rahe J. Volume 2. Dordrecht, The Netherlands: Kluwer Academic Publishers. pp. 1075–1092.

Keller L. P., Thomas K. L., Bradley J. P., and McKay D.S. 1995. Nitrogen in interplanetary dust particles (abstract). *Meteoritics & Planetary Science* 30:526–527.

Keller L. P., Bajt S., Baratta G. A., Borg J., Bradley J. P., Brownlee D. E., Busemann H., Brucato J. R., Burchell M., Colangeli L., D'Hendecourt L., Djouadi Z., Ferrini G., Flynn G., Franchi I. A., Fries M., Grady M. M., Graham G. A., Grossemy F., Kearsley A., Matrajt G., Nakamura-Messenger K., Mennella V., Nittler L., Palumbo M. E., Stadermann F. J., Tsou P., Rotundi A., Sandford S. A., Snead C., Steele A., Wooden D., and Zolensky M. 2006. Infrared spectroscopy of comet 81P/Wild 2 samples returned by Stardust. *Science* 314:1728–1731.

Kissel J., Krueger F. R., Silén J., and Clark B. C. 2004. The Cometary and Interstellar Dust Analyzer at comet 81 P/Wild 2. *Science* 304:1774–1776.

Larimer J. W. 1968. An experimental investigation of oldhamite, CaS; and the petrologic significance of oldhamite in meteorites. *Geochimica et Cosmochimica Acta* 32:965–982.

Lellouch E., Crovisier J., Lim T., Bockelée-Morvan D., Leech K., Hanner M. S., Altieri B., Schmitt B., Trotta E., and Keller H. U. 1998. Evidence for water ice and estimate of dust production rate in comet Hale-Bopp at 2.9 AU from the Sun. *Astronomy and Astrophysics* 339:L9–L12.

Lodders K. and Fegley B. Jr. 1998. *The planetary scientist's companion*. Oxford: Oxford University Press. 371 p.

Mastalerz M. and Gurba L. W. 2001. Determination of nitrogen in coal macerals using electron microprobe technique—Experimental procedure. *International Journal of Coal Geology* 47:23–30.

Matrajt G., Taylor S., Flynn G., Brownlee D., and Joswiak D. 2003. A nuclear microprobe study of the distribution and concentration of carbon and nitrogen in Murchison and Tagish Lake meteorites, Antarctic micrometeorites, and IDPs: Implications for astrobiology. *Meteoritics and Planetary Science* 38:1585–1600.

McKay C. P. and Borucki W. J. 1997. Atmospheric composition and organic production: Early cometary bombardment (abstract). *Bulletin of the American Astronomical Society* 29: 1031.

Mosbah M., Bastoul A., Cuney M., and Pironon J. 1993. Nuclear microprobe analysis of ^{14}N and its application to the study of ammonium-bearing minerals. *Nuclear Instruments and Methods in Physical Research B* 77:450–456.

NIST Standard Database Number 69. 2005. National Institute of Standards and Technology, http://webbook.nist.gov/chemistry. Last accessed February 15, 2008.

Oró J. 2000. Organic matter and the origin of life in the solar system. In: *A new era in bioastronomy*, edited by Lemarchand G. and Meech K. ASP Conference Series, vol. 213. pp. 285–299.

Pizzarrello S., Cooper G. W., and Flynn G. J. 2006. The nature and distribution of the organic material in carbonaceous chondrites and interplanetary dust particles. In: *Meteorites and the early solar system* edited by Lauretta D. S. and McSween H. Y. Jr., Tucson, Arizona: The University of Arizona Press. pp. 625–651.

Sandford S. A., Aléon J., Alexander C. M. O'D., Araki T., Bajt S., Barratta G. A., Borg J., Bradley J. P., Brownlee D. E., Brucato J. R., Burchell M. J., Busemann H., Butterworth A., Clemett S. J., Cody G., Colangeli L., Cooper G., D'Hendecourt L., Zahia D., Dworkin J. P., Ferrini G., Fleckenstein H., Flynn G. J., Franchi I. A., Fries M., Gilles M. K., Glavin D. P., Gounelle M., Grossemy F., Jacobsen C., Keller L. P., Kilcoyne A. L. D., Leitner J., Matrajt G., Meibom A., Mennella V., Mostefaoui S., Nittler L. R., Palumbo M. E., Papanastassiou D. A., Robert F., Rotundi A., Snead C. J., Spencer M. K., Stadermann F. J., Steele A., Stephan T., Tsou P., Tyliszczak T., Westphal A. J., Wirick S., Wopenka B., Yabuta N., Zare R. N., and Zolensky M. E. 2006. Organics captured from comet 81P/Wild 2 by the Stardust spacecraft. *Science* 314:1720–1724.

Simpson J. C. B. and Earwaker L. G. 1986. Use of deuteron-induced nuclear reactions for quantitative surface analysis. *Surface and Coatings Technology* 27:41–56.

Tsou P., Brownlee D. E., Sandford S. A., Hörz F., and Zolensky M. E. 2003. Wild 2 and interstellar sample collection and Earth return. *Journal of Geophysical Research*, doi:10.1029/2003JE002109.

Varela M., Bonnin-Mosbah M.-E., Kurat G., and Gallien J.-P. 2003. Nitrogen micro-analysis of glass inclusions in chondritic olivines by nuclear reaction. *Geochimica et Cosmochimica Acta* 67:1255–1265.

Wang X., Xin Xinquan, Chen H., Anbang D., Tai A. P., and Zhang Y. 1986. Studies on thermal stabilities of coordination compounds by gas chromatography. (XII) The decomposition mechanism of potassium hexacyanoferrate (III) ($K_3[Fe(CN)_6]$). *Kexue Tongbao* 31:90–94.

Zolensky M. E., Zega, Yano H., Wirick S., Westphal A. J., Weistberg M. K., Weber I., Warren J. L., Velbel M. A., Tsuchiyama A., Tsou P., Toppani A., Tomioka N., Tomeoka K., Teslich N., Taheri M., Susini J., Stroud R., Stephan T., Stadermann F. J., Snead C. J., Simon S. B., Simionovici A., See T. H., Robert F., Rietmeijer F. J. M., Rao W., Perronnet M. C., Papanastassiou D. A., Okudaira K.,

Ohsumi K., Onishi I., Nakamura-Messenger K., Nakamura T., Mostefaoui S., Mikouchi T., Meibom A., Matrajt G., Marcus M. A., Leroux H., Lemelle L., Le L., Lanzirotti A., Langenhorst F., Krot A. N., Keller L. P., Kearsley A. T., Joswiak D., Jacob D., Ishii H., Harvey R., Hagiya K., Grossman L., Grossman J. N., Graham G. A., Gounelle M., Gillet P., Genge M. J., Flynn G., Ferroir T., Fallon S., Ebel D. S., Zu R. D., Cordier P., Clark B., Chi M., Butterworth A. L., Brownlee D. E., Bridges J. C., Brennan S., Brearley A., Bradley J. P., Bleuet P., Bland P. A., and Bastien R. 2006. Mineralogy and petrology of comet 81P/Wild 2 nucleus samples. *Science* 314: 1735–1739.